Image Denoising Using Context Quantization and Local Linear Regression

Wen Tian[1], **Minjie Chen**[2], **Mantao Xu**[3], **Pasi Fränti**[2] and **Hongyuan Wang**[1]

[1]Department of Electronics and Information Engineering
Huazhong University of Science and Technology
Wuhan, CHINA

[2]School of Computing
University of Eastern Finland
Joensuu, FINLAND

[3]School of Electric Engineering
Shanghai Dianji University,
CHINA

Abstract — A main challenge for image denoising techniques is the damaging of some specific detailed structures or edges that are useful for image application. That is why edge-preserving filtering has advanced as a prevailing topic in medical image and multimedia processing. Conventional edge-preserving filters have exploited a number of morphological operators and estimated order statistics in a set of variable local windows such that they both enhance the significant edge details and smooth additive and multiplicative noises meanwhile. However, they fail to take into account the importance of weak edges, and therefore treat them as additive or multiplicative noises to be reduced. To overcome this difficulty, we present a efficient image denoising algorithm by using context quantization and local linear regression techniques. The context quantization was conducted according to minimization of conditional entropy of the GAP prediction residual in quantized cells and the local texture features hidden in the contexts. In order to design a robust filter for pixels in each quantized context, the local linear regression technique has been applied. The experimental results validated that the proposed image denoising algorithm outperformed the conventional edge-preserving filters reviewed in this work.

Keywords - *edge-preserving filter, image denoising, context quantization, regression analysis*

I. INTRODUCTION

In recent years, edge-preserving filtering has received a considerable interest in the context of denoising digital images, for example, medical images. Many of medical images are presented in high resolution for the sake of reliable clinical diagnosis. However, their image qualities are often offset by a variety of undesirable noises caused by image acquisition [1]. For instance, the use of low-dose radiation in medical examination may incur a poor image quality degraded by severe multiplicative noises and low image contrast [2]. In particular, the presence of speckle noises in medical images (e.g., ultrasonic images) is due to an image acquisition process via coherent radiation [3]. Of course, the image quality degradation poses an interference and distraction to clinical diagnosis. Thus, it is a common practice in clinical situations to process the image with certain denoising techniques before clinical interpretation. In other words, smoothing filters must be exploited to noise reduction, which, conventionally, can be designed via a fixed-size context or using local windows adaptively [4]. However, the edge details or anatomical structures of interest may be over-blurred and therefore their visual presentations are degraded in contrast when those conventional denoising techniques (e.g., homomorphic filters and polynomial filters) are applied. Eventually, such contrast distortion may lead to severe false recognitions of anatomical structures in clinical practice.

To address this operational issue, a class of nonlinear filters [5-8], edge preserving filters, have been investigated and developed to enhance the so-called signal-to-noise ratio (SNR) whereas the useful edge information must be preserved meanwhile. A number of best practices for edge-preserving smoothing of digital images have been conducted by using order statistic filters [9], bilateral filtering [10], anisotropic diffusion [11] and Bayesian based approach [12-13] and morphological analysis [14]. But a challenge for those edge-preserving filters is, most likely, that they are designed for additive white Gaussian noises [15], which is not acceptable for the image corrupted by impulse noises.

Motivated by the high cost of missing the anatomical details of importance in noise reduction for medical images, a number of edge-preserving filters have been well studied and developed [16-21]. Likewise, the edge-preserving filters have recently been exploited to benefit of advanced medical imaging application, for example, the computer-aided diagnosis system [22]. Our primary objective is to design an adaptive image filter that preserve weak edges containing the edge details of great importance in noise reduction for medical images. However, the main challenge of noise reduction for medical images is that the model parameters for noises are seldom known and difficult to estimate since they do not always obey a fixed distribution. This complexity constraint necessitates the use of universal context modeling or context quantization approach in image compression domain to design an adaptive image filter, in which the distribution of input signal does not need to be known beforehand. In this contribution, we have presented an efficient algorithm to design an edge-preserving filter in terms of regression analysis of neighborhood according to different quantized contexts and multi-band image enhancement techniques. The remainder of this work is organized as follows: In section 2, we introduced context quantization algorithm for estimating filtering coefficients by using regression analysis. The third section deals with the multi-band enhancement techniques for noise reduction and edge enhancement. In section 4, we evaluate the proposed edge-preserving filtering technique over three sets of medical

978-1-4244-6878-2/10/$26.00 ©2010 IEEE

images in a comparison to Gaussian filters and anisotropic diffusion filters. Finally, a conclusion is drawn in section 5.

II. A CONTEXT QUANTIZATION ESTIMATOR

A. Gradient-adjusted predictor

Gradient-adjusted predictor (GAP), proposed by Wu et al [23], is a nonlinear predictor that uses the surrounding pixels to predict the pixel value in the kernel center. It was designed to be adaptive to the image gradients near the predicted pixel. In image coding application, only one side pixels (180°) are used in the prediction in [23]. We modify GAP here so that both sides (360°) of the neighboring pixels are utilized.

$\mathbf{I}_{(i-2,j-2)}$	$\mathbf{I}_{(i-2,j-1)}$	$\mathbf{I}_{(i-2,j)}$	$\mathbf{I}_{(i-2,j+1)}$	$\mathbf{I}_{(i-2,j+2)}$
$\mathbf{I}_{(i-1,j-2)}$	$\mathbf{I}_{(i-1,j-1)}$	$\mathbf{I}_{(i-1,j)}$	$\mathbf{I}_{(i-1,j+1)}$	$\mathbf{I}_{(i-1,j+2)}$
$\mathbf{I}_{(i,j-2)}$	$\mathbf{I}_{(i,j-1)}$	$\mathbf{I}_{(i,j)}$	$\mathbf{I}_{(i,j+1)}$	$\mathbf{I}_{(i,j+2)}$
$\mathbf{I}_{(i+1,j-2)}$	$\mathbf{I}_{(i+1,j-1)}$	$\mathbf{I}_{(i+1,j)}$	$\mathbf{I}_{(i+1,j+1)}$	$\mathbf{I}_{(i+1,j+2)}$
$\mathbf{I}_{(i+2,j-2)}$	$\mathbf{I}_{(i+2,j-1)}$	$\mathbf{I}_{(i+2,j)}$	$\mathbf{I}_{(i+2,j+1)}$	$\mathbf{I}_{(i+2,j+2)}$

Figure 1. 5×5 kernel used in gradient-adjusted prediction

We define the following two quantities.

$$d_h = (|I_{(i,j-2)} - I_{(i,j-1)}| + |I_{(i-1,j-1)} - I_{(i-1,j)}| + |I_{(i-1,j)} - I_{(i-1,j+1)}| + |I_{(i,j+1)} - I_{(i,j+2)}| + |I_{(i+1,j)} - I_{(i+1,j+1)}| + |I_{(i+1,j-1)} - I_{(i+1,j)}|)/2 \quad (1)$$

$$d_v = (|I_{(i-1,j-1)} - I_{(i,j-1)}| + |I_{(i-2,j)} - I_{(i-1,j)}| + |I_{(i-2,j+1)} - I_{(i-1,j+1)}| + |I_{(i-1,j+1)} - I_{(i,j+1)}| + |I_{(i+1,j)} - I_{(i+2,j)}| + |I_{(i+1,j-1)} - I_{(i+2,j-1)}|)/2 \quad (2)$$

where d_h and d_v both consist of six absolute differences and are respectively used to estimate the gradients of the intensity function near pixel $I(i,j)$ in the horizontal and vertical directions. We adopt the gradient-adjusted prediction of an image below:

If $d_v(i,j)-d_h(i,j) > C_1$ {sharp horizontal edge}

$$\hat{I}(i,j) = \frac{I(i,j-1) + I(i,j+1)}{2};$$

Else if $d_v(i,j)-d_h(i,j) < -C_1$ {sharp vertical edge}

$$\hat{I}(i,j) = \frac{I(i-1,j) + I(i+1,j)}{2}$$

Else

$$\hat{I}(i,j) = \frac{I(i,j-1)+I(i,j+1)+I(i-1,j)+I(i+1,j)}{4} + \frac{I(i-1,j+1)-I(i-1,j-1)}{8} + \frac{I(i+1,j-1)-I(i+1,j+1)}{8}$$

If $d_v(i,j)-d_h(i,j) > C_2$ {horizontal edge}

$$\hat{I}(i,j) = \frac{\hat{I}(i,j)}{2} + \frac{I(i,j-1) + I(i,j+1)}{4}$$

Else if $d_v(i,j)-d_h(i,j) > C_3$ {weak horizontal edge}

$$\hat{I}(i,j) = \frac{3\hat{I}(i,j)}{4} + \frac{I(i,j-1) + I(i,j+1)}{8}$$

Else if $d_v(i,j)-d_h(i,j) < -C_2$ {vertical edge}

$$\hat{I}(i,j) = \frac{\hat{I}(i,j)}{2} + \frac{I(i-1,j) + I(i+1,j)}{4}$$

Else if $d_v(i,j)-d_h(i,j) < -C_3$ {weak vertical edge}

$$\hat{I}(i,j) = \frac{3\hat{I}(i,j)}{4} + \frac{I(i-1,j) + I(i+1,j)}{8}$$

End

End

The predictor coefficients and thresholds given above were empirically chosen as $C_1 = 80$, $C_2 = 32$ and $C_3 = 8$. Here $\hat{I}$ represents the prediction result. The variance of prediction errors $e = I - \hat{I}$ strongly correlates to the smoothness of the image around the predicted pixel. In order to model this correlation, an error energy estimator Δ is defined as follows.

$$\Delta = d_h + d_v + |e_{i-1,j}| + |e_{i+1,j}| \quad (3)$$

The definitions of d_h and d_v are given by equation (1) and (2), and

$$e_{i-1,j} = I(i-1,j) - \hat{I}(i-1,j), e_{i+1,j} = I(i+1,j) - \hat{I}(i+1,j)$$

are respectively the left and right prediction errors. $e_{i-1,j}$ and $e_{i+1,j}$ are only included here in Δ because large errors tend to occur consecutively.

By conditioning the error distribution on Δ, the prediction errors can be separated into classes of different variances. We quantize Δ to 4 levels and denote the quantizer as $Q(\Delta) \in \{0,1,2,3\}$. The quantization criterion is to minimize the conditional entropy of the errors. Dynamic programming is used to determine q_1, q_2, q_2, q_3, and q_4, such that $0 = q_1 < q_2 < q_2 < q_2 < q_4 = \infty$, partitions Δ into to 4 intervals so that following function is minimized.

$$-\sum_{d=0}^{3} \sum_{q_d \le \Delta < q_{d+1}} p(e | q_d \le \Delta < q_{d+1}) \log p(e | q_d \le \Delta < q_{d+1}) \quad (4)$$

B. Context Selection

Gradient alone cannot adequately characterize some of the more complex relationships between the predicted pixel $I(i,j)$ and its neighbors. We use a local neighborhood of pixels to form a casual context C of the predicted pixel as follows:

$$C = \{x_0, x_1, x_2, x_3, x_4, x_5, x_6, x_7\} = \{I(i-1,j-1), I(i-1,j), I(i-1,j+1), I(i,j-1), I(i,j+1), I(i+1,j-1), I(i+1,j), I(i+1,j+1)\} \quad (5)$$

Plus, the causal context C can be quantized or modeled by using an 8-bit binary value, $S = s_7 s_6 s_5 s_4 s_3 s_2 s_1 s_0$

$$s_k = \begin{cases} 0 & x_k \geq \hat{I}(i,j) \\ 1 & x_k < \hat{I}(i,j) \end{cases} \qquad 0 \leq k \leq 7 \tag{6}$$

where s captures the texture patterns in the modeling context which are indicative of the behavior of e and the number of different contexts is $2^8 = 256$. Combining $Q(\Delta)$ and S, we obtain $4 \cdot 2^8 = 1024$ different compound contexts in error modeling.

C. Locally Linear Regression Analysis

Each pixel corresponds to one of the 1024 quantized contexts or cells of contexts. This makes it easy to categorize each pixel into 1024 groups according to their quantized contexts. For each pixel belonging to the same specific group, we use all of its neighboring pixel values in a diamond-shape window to predict its value, as shown in figure 2. The predicted pixel value is the weighted sum of all the neighboring pixels values.

$$\sum_{k=1}^{12} b_k x_k + \alpha = y \tag{7}$$

where parameter b_k and α can be obtained from regression analysis. But for achieving robustness of image intensity surface smoothing from noise data [27], locally linear regression is exploited. It combines the advantage of of removing noise in continuity regions and the advantage preserving useful weak edges at the same time. More importantly, a conventional linear regression will introduce a severe estimator bias when smoothing image intensity in a local neighborhood or a context from observation data.

We adopt a training process to estimate the set of locally liner regression parameters for each pixel group, where 1024 sets of parameters can be achievable. Images used in the training process consist of two groups: A and B. Images in

		x_1		
	x_2	x_3	x_4	
x_5	x_6	y	x_7	x_8
	x_9	x_{10}	x_{11}	
		x_{12}		

Figure 2. pixels used in locally linear regression analysis

group A are original (noise free) images while images in group B are the noise corrupted images. The prediction of all the pixels in a quantized context can be done using a kernel linear combination or filter

$$y(\mathbf{X}_0) = \mathbf{X}_0 \beta(\mathbf{X}_0) + \alpha(\mathbf{X}_0) \tag{8}$$

where we have

$$\mathbf{X}_0 = (x_1, \cdots, x_{12}), \qquad \beta = (b_1, \cdots, b_{12}) \tag{9}$$

and $y(\mathbf{X}_0)$ is an estimator for minimizing

$$\min_{\alpha(\mathbf{X}_0), \beta(\mathbf{X}_0)} = \sum_{i=1}^{N_{Q(C)}} K(\mathbf{X}_0, \mathbf{X}_i)(y(\mathbf{X}_i) - \mathbf{X}_0 \beta(\mathbf{X}_0) + \alpha(\mathbf{X}_0))^2 \tag{10}$$

and K is a mercer kernel function. Estimating β and α needs an adequate number of training images since the context based filter in (8) will use different parameters β and α for each of 1024 quantized contexts. As desired, these parameters can be saved in off-line and used to process similar images used in the

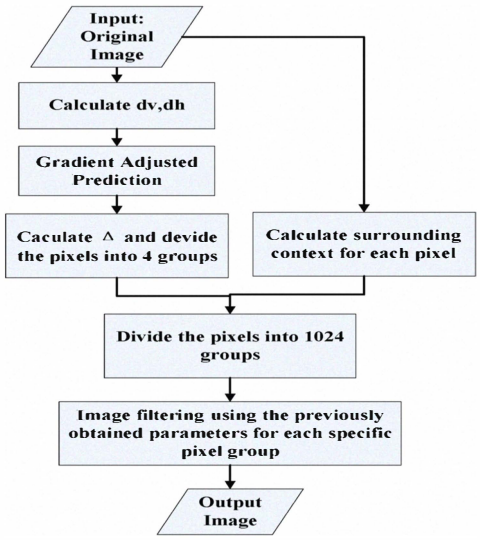

Figure 3. workflow of image pixel predication

training procedure. Otherwise, one need to optimize the parameters for each quantized contexts for the noisy image directly but this would lead to a context dilution problem. The proposed context quantization-based filtering (CQF) image denoising algorithm is illustrated in fig. 3.

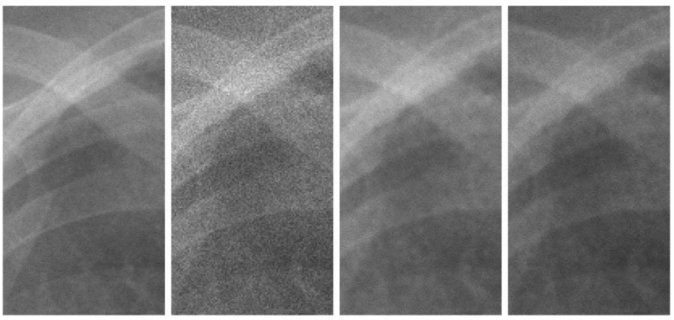

Figure 4. Filtering on Chest X-ray image, from left to right: a) original image b) noised image c) CQF d) M-CQF

III. MULTI-BAND EDGE ENHANCEMENT

In order to further enhance the edges in the image, we design a multi-band edge enhancing process incorporating the context quantization based filters and *Gaussian* filters, which is shown in figure 4. CQF and Gaussian filters are both applied to images sampled with three different sizes, namely, the original size, 1/4 size and 1/16 size. The differences between images processed by the two methods are multiplied by a coefficient and then added to the Gaussian filtered image to form the

output image. Empirically, the values of coefficients K_1, K_2 and K_3 are respectively assigned 1.3, 0.4 and 0.1. The size of the two dimensional *Gaussian* filter is 5 by 5 and the sigma value of Gaussian filters is 2.0.

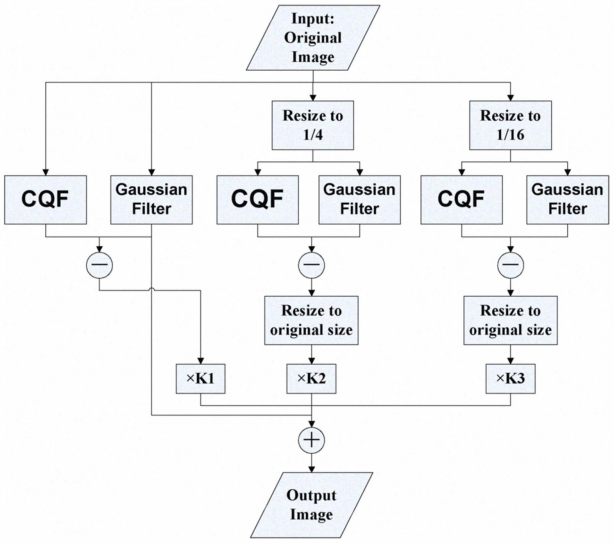

Figure 5. Diagram of multiband context quantization bsaed filter

IV. EXPERIMENT RESULTS

The performance of the proposed *Context Quantization Based* filter (CQF) and Multiband CQF methods with DR chest X-ray images and brain T1 MRI images are evaluated in this section. *Gaussian* filter, *anisotropic* diffusion filters with n number of iterations (AD_1~AD_5 where n = 1,…,5) [11] and *mean of least variance* filter (MLV) [28] are also studied as performance benchmark. Each case of Chest X-ray images and MRI images has a noise-free image and several noise corrupted images with different noise levels. Both objective and subject image quality measurements are used in performance evaluations. *Peak Signal-to-Noise Ration* (PSNR) and *Structural Similarity index* (SSIM) [25] between the noise-free images and the processed noised images are the objective measurements. The PSNR of image X and Y with size = MN is defined by:

$$PSNR = 10\log_{10}(\frac{MAX_X^2}{MSE(X,Y)}) = 20\times\log_{10}((\frac{MAX_X}{MSE(X,Y)})) \quad (11)$$

in which MAX_I is the maximum possible pixel value of image I and MSE is defined by

$$MSE(X,Y) = \frac{1}{mn}\sum_{i=0}^{m-1}\sum_{j=0}^{n-1}\left\|X(i,j)-Y(i,j)\right\|^2 \quad (12)$$

whereas SSIM metric is calculated on various windows of an image. The measure between two windows of the size $N\times N$ x and y is

$$SSIM(X,Y) = \frac{(2\mu_X\mu_Y + c_1)(2cov_{XY} + c_2)}{(\mu_X^2 + \mu_Y^2 + c_1)(\sigma_X^2 + \sigma_Y^2 + c_2)} \quad (13)$$

where μ_X and μ_Y are the average values of image X and Y, respectively, σ_X^2 and σ_Y^2 are the variance of the same images, and cov_{XY} is the covariance of image X and Y. And $c_1 = (k_1L)^2$ and $c_2 = (k_2L)^2$ are two variables used to stabilize the division with weak denominator, L is the dynamic of the pixel-values, $k_1 = 0.01$ and $k_2 = 0.03$ by default.

For subjective indicators, a panel of clinician was invited to evaluate image quality for the testing images before and after noise-reductions using a subjective rating from 1 to 10 (A higher rating indicates the better quality while lower rating represents a worse image quality). In order to compare the performance of those different filters on fairness, the parameters of the filters are adjusted so that they can achieve their best visual performance on the images being processed.

A. Chest X-ray image

The original digital Chest X-ray images are carefully examined and they are in good image quality. Hence they can be viewed as noise free image. We include 10 number of Chest X-ray images to form group *A* and add *Gaussian* noise to the same set of images to construct group *B*. We conduct our experiments on these images generated by a wide range of Gaussian noise density levels—$0.0001 \leqslant \sigma \leqslant 0.0011$ with an increment step of 0.0002. The parameters obtained from the training process are used to process the noise-corrupted images with the same level of *Gaussian* noise as that of the noised images used in training. The mean PSNR and SSIM indexes associated with the processed images and the noised images are shown in Fig. 6 and Fig. 7.

It turns out that the PSNRs obtained by the seven noise reduction methods are significantly different. Anisotropic diffusion filters achieve the best result while MLV filter provides the worst performance for the images corrupted by 0.01-0.07% noises. CQF filter is inferior to the anisotropic diffusion filters for the images with lower noises, whereas performs better than them with increased noises. The performance of CQF seems to be more robust to high noise level than anisotropic filters. Similar conclusions can be drawn in terms of SSIM measurements. In subjective evaluation, M-CQF is rated as the highest due to its edge enhancing effect, and CQF ranks the second subsequently. T-test on subjective ratings has revealed that the M-CQF perform statistically better than other filters are reviewed over the Chest X-ray images.

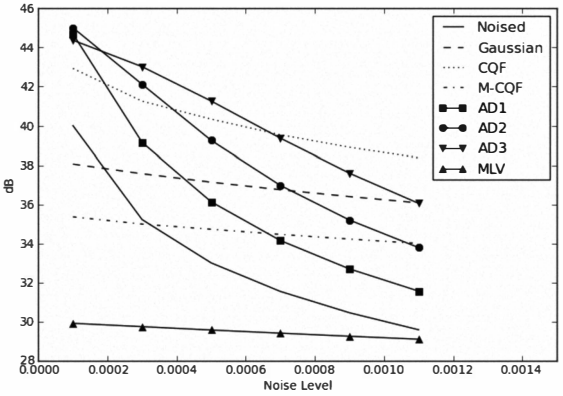

Figure 6. PSNR evaluation for Chest X-ray images

B. *Brain MRI images*

The brain MRI images are downloaded from a database provided by McGill University of Canada [26]. This database provides brain MRI images and noised versions of those images of 5 different noise levels, namely, 1%, 3%, 5%, 7% and 9%. The noises in the simulated images obey *Rayleigh* distribution in the background and *Rician* statistics in the signal regions respectively. The "percent noise" number represents the percent ratio of the standard deviation of the white *Gaussian* noise versus the signal for a reference tissue. Those images are handled in the same ways as the Chest X-ray images and similar conclusions can be drawn from Fig. 11-12.

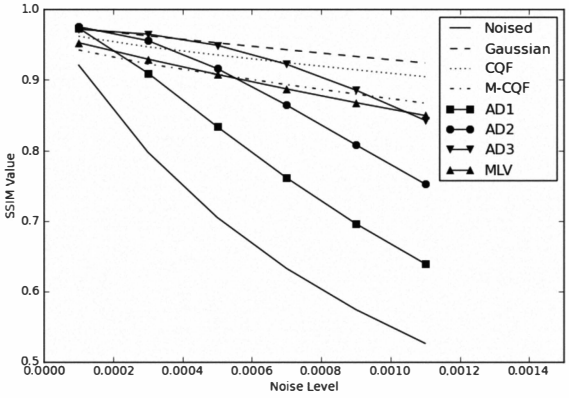

Figure 7. SSIM evaluation for Chest X-ray images

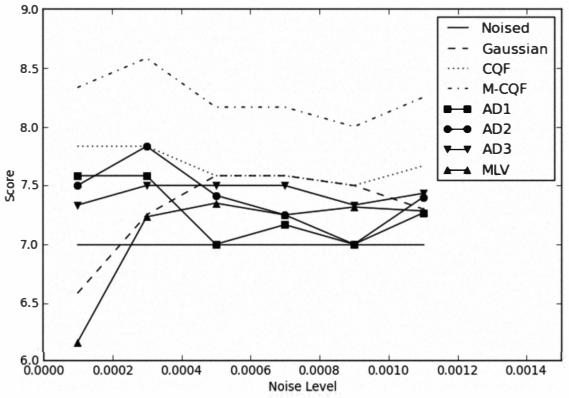

Figure 8. Subjective evaluation for Chest X-ray images

V. CONCLUSION

In this paper, an efficient edge preserving image filtering algorithm is proposed. The pixels in the images are divided into 1024 groups according to each pixel's Δ value and their compound contexts. For each group of pixels, we apply locally linear regression to estimation of filtering coefficients. The effectiveness of this method is evaluated in a performance comparison to the other two edge preserving filters and *Gaussian* filters. Subjective and objective experimental performance studies have demonstrated that the underlying context quantization based image denoising technique is superior to the other methods also studied in this work.

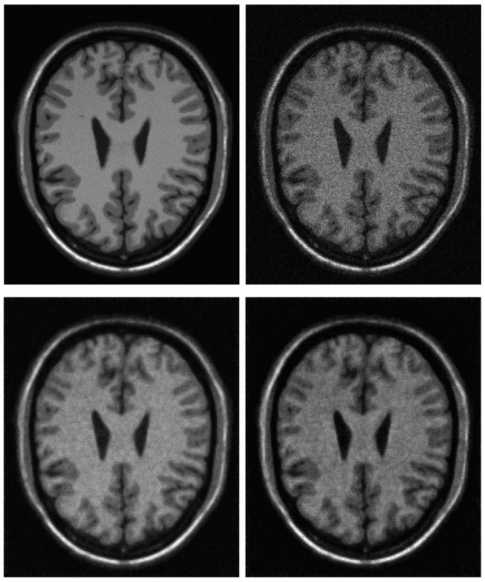

Figure 9. Filtering on MRI image, from left to right: a) original image b) noised image c) CQBF d) MCQBF

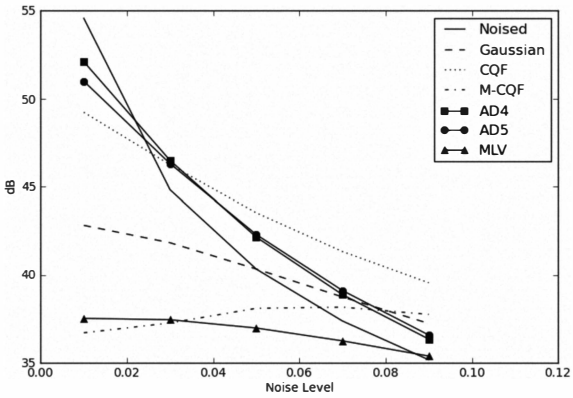

Figure 10. PSNR evaluation for MRI Images

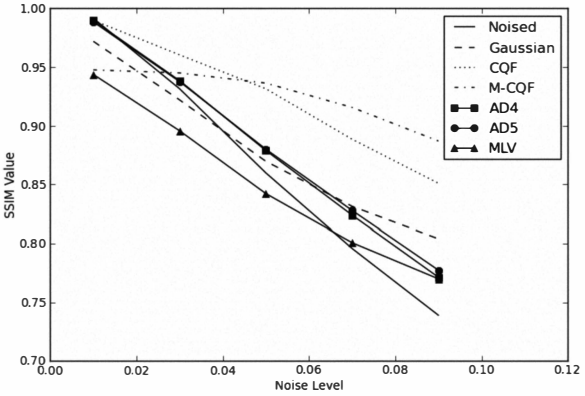

Figure 11. SSIM evaluation for MRI images

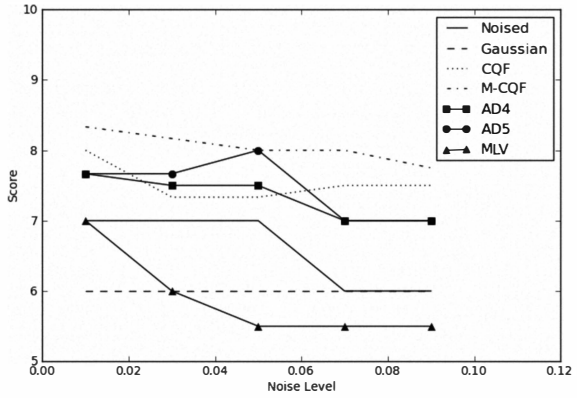

Figure 12. Subjective evaluation for MRI images

REFERENCES

[1] I.E. Abdou and N.J. Dusaussoy, "Survey of image quality measurements", in Proceedings of 1986 ACM Fall joint computer conference, pp.71 – 78, Nov. 1986.

[2] M. Hensel, U. Brummund, T. Pralow and R. Grigat, "Noise Reduction with Edge Preservation by Multi-scale Analysis of Medical X-Ray Image Sequences", in Proceedings of BVM 2005.

[3] C.B. Burckhardt, "Speckle in Ultrasound B-Mode Scans", IEEE Transactions on Sonics and Ultrasonics, 25(1), pp.1-6, Jan 1978.

[4] L. Yang, S. Li, X. Lu and Z. Guo, "A new approach to select the optimum neighborhood for edge preserving filter", pp.96-99, in Proceedings of the Fourth International Conference on Image and Graphics, Chengdu, China, August 2007.

[5] R. Wang, J. L. Lin, D. Y. Li and T. F. Wang, "Edge Enhancement and Filtering of Medical Ultrasonic Images Using a Hybrid Method", The 1st International Conference on Bioinformatics and Biomedical Engineering (ICBBE 2007), pp.876–879, Wuhan, China, 6-8 July 2007.

[6] Y. Chen, R. Yin, P. Flynn and S. Broschat, "Aggressive region growing for speckle reduction in ultrasound images", Pattern Recognition Letters, 24(4), pp.677-691, 2003.

[7] K. Krajsek and R. Mester, "The Edge Preserving Wiener Filter for Scalar and Tensor Valued Images", 28th Annual Symposium of the German Association for Pattern Recognition (Lecture Notes in Computer Science), Springer Berlin / Heidelberg, 4174, pp.91-100, 2006.

[8] S. Luo and J. Han, "Filtering Medical Image Using Adaptive Filter", 23rd Annual International Conference of the IEEE Engineering in Medicine and Biology Society (EMBS 2001), vol. 3, pp.2727-2729, 25-28 Oct. 2001.

[9] P.K Sinha and Q. Hong, "An improved median filter", IEEE Transactions on Medical Imaging, 9(3), pp.345 – 346, Sept 1990.

[10] M. Elad, "On the origin of the bilateral filter and ways to improve it", IEEE Transactions on Image Processing, 11(10), pp.1141-1151, Oct 2002.

[11] S.L. Keeling, "Total variation based convex filters for medical imaging", Applied Mathematics and Computation, 139(1), pp.101-119, July 2003.

[12] C. Bouman and K. Sauer, "A generalized Gaussian image model for edge-preserving MAP estimation", IEEE Transactions on Image Processing, 2(3), pp.296-310, July 1993.

[13] J.M. Sanches, J.C. Nascimento and J.S. Marques, "Medical Image Noise Reduction Using the Sylvester–Lyapunov Equation", Image Processing, IEEE Transactions on Medical Imaging, 17(9), pp.1522-1539, Sept. 2008.

[14] M.A. Schulze, Biomedical Image Processing with Morphology-Based Nonlinear Filters, Ph.D. Dissertation, The University of Texas at Austin, 1994.

[15] J.A. Lee, X. Geets, V. Gregoire and A. Bol, "Edge-Preserving Filtering of Images with Low Photon Counts", IEEE Transactions on Pattern Analysis and Machine Intelligence, 30(6), pp. 1014 – 1027, June 2008.

[16] A. Goshtasby and M. Satter, "An adaptive window mechanism for image smoothing", Computer Vision and Image Understanding, 111(2), pp. 155-169, August 2008.

[17] C.K. Chu, I. K. Glad, F. Godtliebsen and J.S. Marron, "Edge-preserving smoother for image processing", Journal of the American Statistical Association, 93(442), pp.526-541, June1998.

[18] M. Ceccarelli, "A Finite Markov Random Field approach to fast edge-preserving image recovery", Image and Vision Computing, 25(6), pp.792-804, June 2007.

[19] M. Welk, J. Weickert, F. Becker, C. Schnorr, C. Feddern and B. Burgeth, "Median and related local filters for tensor-valued images", Signal Processing, 87 (2), pp. 291-308, Feb. 2007.

[20] B.W. Reutter, V.R. Algazi and R.H. Huesman, "Computationally efficient nonlinear edge preserving smoothing of n-D medical images via scale-space fingerprint analysis", in 2000 IEEE Nuclear Science Symposium and Medical Imaging Conference, vol. 2, pp. 282-286, Lyon, France, October 2000.

[21] K. Krajsek and R. Mester, "The Edge Preserving Wiener Filter for Scalar and Tensor Valued Images", in Proceedings of 28th DAGM Symposium on Pattern Recognition, pp. 91-100, Berlin, Germany, Sept. 2006.

[22] D. Pilkinton, I. Bitter, R.M. Summers, S. Campbell, R.J. Choi and P.J Pickhardt, "The Effect of Edge-Preserving Image Smoothing on Automatic Colonic Polyp Detection for CT Colonography", in Proceedings of SPIE Medical Imaging, vol. 6143, pp. 984-991, San Diego, USA, 2006.

[23] X. Wu and N. D. Memon. Context-Based, Adaptive, Lossless Image Coding. IEEE Transactions of Communications, 1997, 45(4): 437-444.

[24] Mark A S, John A P. Value-and-Criterion Filters: A new filter structure based upon morphological opening and closing, Nonlinear Image Processing IV, Proc. SPIE, 1993, 1902: 106-115.

[25] Z. Wang, A.C. Bovik, H.R. Sheikh and E.P. Simoncelli, Image Quality Assessment: From Error Visibility to Structural Similarity, IEEE Transactions on Image Processing, Vol. 13, No. 4, April 2004.

[26] http://www.bic.mni.mcgill.ca/brainweb.

[27] I. Gijbels, A. Lambert, and P. Qiu, "Edge-Preserving Image Denoising and Estimation of Discontinuous Surfaces," IEEE Transactions on PAMI, Vol. 28 , Issue 7 table of contents. pp. 1075 – 1087, July 2006.

[28] *M. A. Schulze* and J. A. Pearce, "Value-and-criterion filters: a new filter structure based upon morphological opening and closing," in *E. R. Dougherty, J. Astola, and H. Longbotham, eds., Nonlinear Image Processing IV. Proc. SPIE, v. 1902 (1993)*, pp. 106-115, San Jose, California, Feb. 1993